

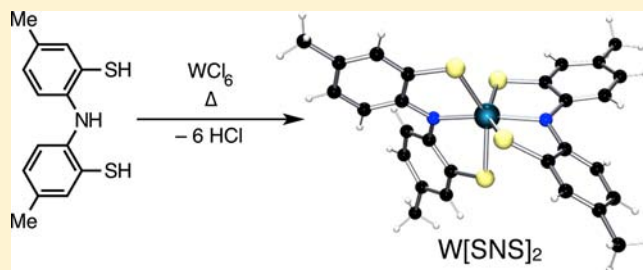
Synthesis and Characterization of a Redox-Active Bis(thiophenolato)amide Ligand, $[\text{SNS}]^{3-}$, and the Homoleptic Tungsten Complexes, $\text{W}[\text{SNS}]_2$ and $\text{W}[\text{ONO}]_2$

David W. Shaffer, Géza Szigethy, Joseph W. Ziller, and Alan F. Heyduk*

Department of Chemistry, University of California, Irvine, California, 92697, United States

Supporting Information

ABSTRACT: A new tridentate redox-active ligand platform, derived from bis(2-mercapto-*p*-tolyl)amine, $[\text{SNS}^{\text{cat}}]_3\text{H}_3$, has been prepared in high yields by a four-step procedure starting from commercially available bis(*p*-tolyl)amine. The redox-active pincer-type ligand has been coordinated to tungsten to afford the six-coordinate, homoleptic complex $\text{W}[\text{SNS}]_2$. To benchmark the redox behavior of the $[\text{SNS}]$ ligand, the analogous tungsten complex of the well-known redox-active bis(3,5-di-*tert*-butylphenolato)amide ligand, $\text{W}[\text{ONO}]_2$, also has been prepared. Both complexes show two reversible reductions and two partially reversible oxidations. Structural, spectroscopic, and electrochemical data all indicate that $\text{W}[\text{ONO}]_2$ is best described as a tungsten(VI) metal center coordinated to two $[\text{ONO}^{\text{cat}}]^{3-}$ ligands. In contrast, experimental data suggests a higher degree of S→W π donation, giving the $\text{W}[\text{SNS}]_2$ complex non-innocent electronic character that can be described as a tungsten(IV) metal center coordinated to two $[\text{SNS}^{\text{sq}}]^{2-}$ ligands.

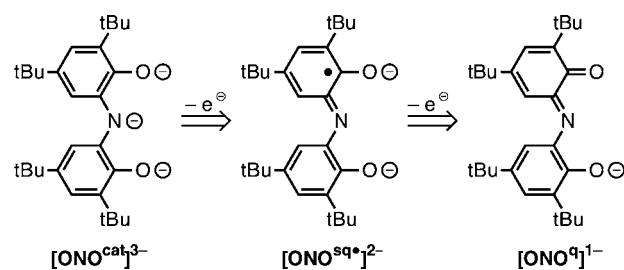


INTRODUCTION

Metal complexes containing redox-active ligands with a tridentate, pincer-type architecture have received increased attention recently owing to their intriguing electronic properties and rich reactivity.^{1–4} Pincer-type ligands offer a robust, meridional coordination environment for the binding of transition metal ions and can include both hard donor atoms such as oxygen and nitrogen and soft donor atoms such as sulfur and phosphorus. With regard to redox-active ligands, the pincer motif is advantageous because the tridentate coordination prevents ligand dissociation during oxidation state changes to the ligand; furthermore, the meridional coordination mode helps to maintain a planar geometry allowing redox-changes to be delocalized over the entire ligand framework. The delocalized nature of the redox-active ligand orbitals may also help to avoid the kinetic barriers associated with geometric rearrangements that occur for localized changes to metal oxidation states. Examples of redox-active, pincer-like ligands include bis(imino)pyridines,³ bis(phosphino)pyridines and amides, bis(anilido)amides,¹ and various other tridentate ligands.^{5–7} Metal complexes supported by such ligands have shown promise in promoting multielectron reactions, and warrant the development of new redox-active pincer-type ligand platforms.

One of the best studied redox-active pincer ligands is the $[\text{ONO}]$ platform, derived from bis(3,5-di-*tert*-butylphenol)-amine $[\text{ONO}^{\text{cat}}]_3\text{H}_3$.^{8–15} The $[\text{ONO}]$ ligand has been characterized in three oxidation states when coordinated to metal ions (Chart 1): the fully reduced catechol trianion $[\text{ONO}^{\text{cat}}]^{3-}$, the dianionic, radical semiquinonate, $[\text{ONO}^{\text{sq}}]^{2-}$,

Chart 1



and the monoanionic iminoquinonate, $[\text{ONO}^{\text{q}}]^{-1}$.¹ While homoleptic complexes with the formulation $\text{M}[\text{ONO}]_2$ were originally synthesized by the aerobic condensation of NH_3 with 3,5-di-*tert*-butylcatechol in the presence of divalent metal salts,¹¹ more recently, the synthesis, characterization, and reactivity of metal complexes containing a single $[\text{ONO}]$ ligand have been elucidated by way of isolated $[\text{ONO}^{\text{cat}}]_3\text{H}_3$ or $[\text{ONO}^{\text{q}}]\text{K}$.^{16,17}

Another attractive pincer-type ligand platform would be one that preserves the redox-activity of the $[\text{ONO}]$ ligand while incorporating softer donor atoms for metal binding. Given the importance of sulfur-based ligands in both synthetic and biological coordination chemistry, and the long-known non-innocent behavior of transition metal dithiolene complexes,^{18–23} it is surprising that sulfur ligands derived from

Received: November 15, 2012

Published: February 6, 2013



bis(thiophenol)amines, analogous to the [ONO] platform, are not known in the literature. Coordination complexes of bidentate dithiolates and aminothiolates have been well-studied, and a variety of metal complexes containing tridentate sulfur-containing ligands have been described including such motifs as (ONS),²⁴ (ONSR),^{25,26} (NNS),²⁷ (NNRS),²⁸ (NSN),^{29,30} and (RSNSR).³¹ Notably, an (SNMeS) platform has been synthesized,³² but methylation of the central nitrogen donor prevents conjugation, thus reducing the ligand's redox-activity compared to the [ONO] platform.

Described herein is the synthesis of a new redox-active, pincer-type ligand derived from bis(2-mercapto-*p*-tolyl)amine, [SNS^{cat}]₃H₃. Preparation of the ligand precursor relies on a dimethyldisulfide oxidation of a benzyl-protected, dilithium salt of di-*p*-tolylamine, that should be applicable to the preparation of a variety of [SNS] derivatives with different backbone substitution patterns. To benchmark the metal-binding and redox-active properties of the [SNS] platform, the homoleptic W[SNS]₂ complex was prepared and characterized by NMR, UV-vis-NIR, and IR absorption spectroscopies, APCI mass spectrometry, cyclic voltammetry, and X-ray crystallography. For comparison, the previously uncharacterized tungsten complex, W[ONO]₂, was also examined. Both tungsten complexes are neutral, diamagnetic species: W[ONO]₂ is well described as a W^{VI} complex containing two [ONO^{cat}]³⁻ ligands, while W[SNS]₂ has non-innocent character suggestive of a W^{IV} center with two [SNS^{sq}]²⁻ ligands.

EXPERIMENTAL SECTION

General Considerations. Some of the complexes described below are air and moisture sensitive, necessitating that manipulations be carried out under an inert atmosphere of argon or nitrogen gas using standard Schlenk, vacuum-line, and glovebox techniques unless otherwise noted. Hydrocarbon solvents were sparged with nitrogen and then deoxygenated and dried by passage through Q5 and activated alumina columns, respectively. Ethereal and halogenated solvents were sparged with nitrogen and then dried by passage through two activated alumina columns. To test for effective oxygen and water removal, nonchlorinated solvents were treated with a few drops of a purple solution of sodium benzophenone ketyl in tetrahydrofuran (THF).

Electrochemical Methods. Electrochemical experiments were performed on a Gamry Series G 300 Potentiostat/Galvanostat/ZRA (Gamry Instruments, Warminster, PA, U.S.A.) using a 3.0 mm glassy carbon working electrode, a platinum wire auxiliary electrode, and a silver wire reference electrode. Electrochemical experiments were performed at room temperature in a glovebox, under an atmosphere of nitrogen. Electrochemical samples were 1.0 mM analyte solutions in THF or CH₂Cl₂ containing 0.10 M [*n*-Bu₄N][PF₆] as the supporting electrolyte. All potentials were referenced to the [Cp₂Fe]⁺⁰ couple using ferrocene or decamethylferrocene as an internal standard.³³ Ferrocene and decamethylferrocene (Acros) were purified by sublimation under reduced pressure and tetra-*n*-butylammonium hexafluorophosphate (Acros) was recrystallized from ethanol three times and dried under vacuum. To verify that electrode processes were diffusion-controlled, forward peak currents were plotted with respect to the square root of scan rates in the range of 50 to 1600 mV/s and found to be linear.

Physical Methods. NMR spectra were collected on a Bruker Avance 500 MHz spectrometer in dry, degassed C₆D₆. ¹H NMR spectra were referenced to TMS using the residual proteo impurities of the solvent at δ = 7.16 ppm; ¹³C NMR spectra were referenced to TMS using the natural abundance ¹³C impurities of C₆D₆ at δ = 128.4 ppm. All chemical shifts are reported using the standard δ notation in parts per million; positive chemical shifts are to a higher frequency from the given reference. Infrared spectra were recorded as KBr pellets with a Perkin-Elmer Spectrum One FTIR spectrophotometer.

Electronic absorption spectra were recorded with Perkin-Elmer Lambda 800 and 900 UV-vis spectrophotometers in 1-cm quartz cells using dry, degassed CH₂Cl₂. Atmospheric-pressure chemical ionization mass spectrometry (APCI-MS) and electrospray ionization mass spectrometry (ESI-MS) data were collected on a Waters LCT Premier mass spectrometer.

Bis(2-bromo-*p*-tolyl)amine. This compound was synthesized according to a literature preparation, but the reaction proceeded in lower yield, and the final product required an added recrystallization step.³⁴ An effective recrystallization method was found to be dissolution of the solids in a minimum amount of hot EtOH (until no second phase of oil is observed). With continued rapid stirring, the recrystallization flask was transferred to an ice water bath and stirred as it cooled, which seized the solution with a fine white solid. This material was collected by filtration, washed with cold EtOH, and dried under vacuum to yield product usable for the next synthetic step, albeit with significant loss of total yield to about 60–75%.

***N*-benzyl-bis(2-bromo-*p*-tolyl)amine.** A solution of bis(2-bromo-*p*-tolyl)amine (5.84 g, 16.5 mmol, 1 equiv) in 50 mL of THF was frozen, and KH (691 mg, 17.2 mmol, 1.05 equiv) was added upon thawing. The mixture was allowed to warm to room temperature and stirred until gas evolution ceased, giving a yellow, homogeneous solution. The solution was again frozen and immediately upon thawing, benzyl bromide was added (1.96 mL, 16.5 mmol, 1 equiv). This mixture was allowed to warm to room temperature and was then stirred for 2 days to afford a pale yellow suspension. Solvent was removed under vacuum, the residue was coevaporated once with Et₂O, and the solid residue was transferred to a Soxhlet extractor and extracted into 125 mL of Et₂O. Solvent was removed from the yellow extract to yield *N*-benzyl-bis(2-bromo-*p*-tolyl)amine as a white solid (7.13 g, 97%). Analytically pure samples were recrystallized from Et₂O at -4 °C as fine white needles. Anal. Calcd. (Found) for C₂₁H₁₉NBr₂ (%): C, 56.66 (56.86); H, 4.30 (4.30); N, 3.15 (3.14). ¹H NMR (C₆D₆) δ/ppm: 1.82 (s, 6H, CH₃), 4.65 (s, 2H, CH₂), 6.62 (d, *J* = 8.5 Hz, 2H, aryl-H), 6.77 (d, *J* = 8.0 Hz, 2H, aryl-H), 6.95 (t, *J* = 7.5 Hz, 1H, aryl-H), 7.10 (t, *J* = 7.5 Hz, 2H, aryl-H), 7.27 (s, 2H, aryl-H), 7.57 (d, *J* = 8.0 Hz, 2H, aryl-H). ¹³C{¹H} NMR (C₆D₆) δ/ppm: 20.17 (CH₃), 57.12 (CH₂), 121.61 (aryl-C), 125.28 (aryl-C), 127.22 (aryl-C), 127.93 (aryl-C), 128.62 (aryl-C), 134.94 (aryl-C), 135.12 (aryl-C), 138.43 (aryl-C), 145.11 (aryl-C). MS (ESI+) *m/z*: 465.8 (28%, MNa⁺), 467.8 (39%, MNa⁺).

***N*-benzyl-bis(2-methanethio-*p*-tolyl)amine.** A homogeneous solution of *N*-benzyl-bis(2-bromo-*p*-tolyl)amine (7.11 g, 16.0 mmol, 1 equiv) in 180 mL of Et₂O was frozen in a liquid-nitrogen cold well. Immediately upon thawing, a solution of *n*BuLi in hexanes (2.47 M, 12.9 mL, 31.9 mmol, 2 equiv) was added, and the resultant heterogeneous mixture was allowed to warm with stirring until it became homogeneous (ca. 20 min), at which point MeSSMe (2.83 mL, 31.9 mmol, 2 equiv) was added. This mixture became heterogeneous immediately and was stirred overnight at room temperature. The reaction was quenched by the addition of 100 mL of water and 200 mL of CH₂Cl₂. The layers were separated, and the aqueous layer was extracted twice with CH₂Cl₂ (2 × 50 mL). The combined organic layers were washed with water (50 mL) and saturated brine (25 mL) and dried over Na₂SO₄ before the solvent was removed under vacuum. The resultant solid was stirred in 10 mL of Et₂O, filtered, and washed twice with Et₂O (2 × 10 mL) to yield *N*-benzyl-bis(2-methanethio-*p*-tolyl)amine as a white, microcrystalline solid (5.13 g, 81%). Analytically pure samples were recrystallized from Et₂O at -4 °C as fine white needles. Anal. Calcd. (Found) for C₂₃H₂₅NS₂ (%): C, 72.78 (72.42); H, 6.64 (6.61); N, 3.69 (3.65). ¹H NMR (C₆D₆) δ/ppm: 1.94 (s, 6H, CH₃), 2.06 (s, 6H, SCH₃), 4.83 (s, 2H, CH₂), 6.67 (d, *J* = 8.0 Hz, 2H, aryl-H), 6.78 (s, 2H, aryl-H), 6.95–6.96 (m, 3H, aryl-H), 7.13 (d, *J* = 8.0 Hz, 2H, aryl-H), 7.71 (d, *J* = 7.5 Hz, 2H, aryl-H). ¹³C{¹H} NMR (C₆D₆) δ/ppm: 14.28 (SCH₃), 20.03 (CH₃), 56.56 (CH₂), 123.69 (aryl-C), 125.28 (aryl-C), 125.76 (aryl-C), 126.96 (aryl-C), 127.96 (aryl-C), 128.50 (aryl-C), 133.74 (aryl-C), 136.45 (aryl-C), 139.45 (aryl-C), 143.93 (aryl-C). MS (ESI+): *m/z* = 380.1 (100%, MH⁺).

Bis(2-mercapto-*p*-tolyl)amine, [SNS^{cat}]₃H₃. A suspension of *N*-benzyl-bis(2-methanethio-*p*-tolyl)amine (5.03 g, 13.3 mmol) in 60 mL of condensed anhydrous ammonia was stirred in a Schlenk flask and maintained between -70 and -60 °C by cooling in a dry ice/isopropanol bath. Solid sodium metal was added in small pieces, allowing the deep blue color associated with the solvated electron to quench before the addition of the next piece. Once the blue color persisted for 15 min (between 6 and 9 equiv of sodium), the mixture was quenched by the addition of excess NH₄Cl. The liquid ammonia was evaporated under a stream of nitrogen. The residue was dissolved in water, cooled in an ice water bath and treated dropwise with concentrated HCl until pH < 1. The resulting yellow suspension was extracted with Et₂O (2 × 75 mL). The combined organics were washed with water and saturated brine, dried with Na₂SO₄, and the solvent was removed under vacuum. The residual oil was passed through a glass wool filter to remove a small amount of solids, using petroleum ether to collect the last fractions of oil. Residual solvent was removed under vacuum to yield the product as an air-stable, viscous, yellow oil (3.20 g, 92%). ¹H NMR (C₆D₆) δ/ppm: 1.99 (s, 6H, CH₃), 2.95 (s, 2H, SH), 6.19 (s, 1H, NH), 6.70 (d, *J* = 8.0 Hz, 2H, aryl-H), 6.84 (d, *J* = 8.0 Hz, 2H, aryl-H), 7.09 (s, 2H, aryl-H). ¹³C{¹H} NMR (C₆D₆) δ/ppm: δ 20.42 (CH₃), 119.11 (aryl C), 120.50 (aryl-C), 128.86 (aryl-C), 131.64 (aryl-C), 133.87 (aryl-C), 140.58 (aryl C). IR (KBr) $\bar{\nu}_{\text{max}}$ /cm⁻¹: 3340 (N-H), 2525 (S-H). MS (ESI+) *m/z*: 262.0 (MH⁺, 42%).

Synthesis of W[SNS]₂. A dark blue suspension of WCl₆ (162 mg, 408 μmol, 1 equiv) in 10 mL of toluene was treated with a yellow solution of [SNS^{cat}]₃H₃ (219 mg, 837 μmol, 2.05 equiv) in 16 mL of toluene. The resulting dark maroon solution was heated to reflux for 8.5 h. After solvent removal under reduced pressure, the crude product was redissolved in 2 mL of toluene, and 10 mL of pentane was added to induce precipitation of the product. The solid was removed by filtration, washed with 3 × 2 mL of pentane, and dried under reduced pressure to provide the product as a purplish-brown solid in 65% yield (186.1 mg). ¹H NMR (C₆D₆) δ/ppm: 2.14 (s, 12H, -Me), 6.59 (ddd, ³*J*_{HH} = 8.7 Hz, ⁴*J*_{HH} = 1.8 Hz, ⁴*J*_{HH} = 0.5 Hz, 4H, aryl-H), 7.07 (br s, 4H, aryl-H), 7.43 (d, ³*J*_{HH} = 8.6 Hz, 4H, aryl-H). ¹³C{¹H} NMR (C₆D₆) δ/ppm: 20.3 (-Me), 121.3 (aryl-C), 126.5 (aryl-C), 129.3 (aryl-C), 137.3 (aryl-C), 152.0 (aryl-C), 154.2 (aryl-C). APCI-MS (toluene) *m/z*: 697.9 ([M]⁺), 698.9 ([M+H]⁺). UV-vis (CH₂Cl₂) λ_{max} /nm (ε/M⁻¹ cm⁻¹): 461 (19,300), 766 (3,620).

Synthesis of W[ONO]₂. A dark blue suspension of WCl₆ (111 mg, 279 μmol, 1 equiv) in 10 mL of toluene was treated with a colorless solution of [ONO^{cat}]₃H₃ (249 mg, 586 μmol, 2.1 equiv) in 12 mL of toluene. The resulting dark orange solution was stirred for 7 h at room temperature then heated to reflux for 16 h. The solvent was removed under reduced pressure. The crude product was redissolved in 5 mL of toluene and 10 mL of MeCN was added to effect precipitation of the product. The solid was removed by filtration, washed with MeCN (2 × 2 mL) and cold Et₂O (2 × 2 mL), and dried to provide the product as an orange-brown solid in 74% yield (211.8 mg). Anal. Calcd. (Found) for C₅₆H₈₀N₂O₄W (%): C, 65.36 (65.15); H, 7.84 (7.80); N, 2.72 (2.58). ¹H NMR (C₆D₆) δ/ppm: 1.28 (s, 18H, -tBu), 1.40 (s, 18H, -tBu), 6.92 (d, ⁴*J*_{HH} = 1.7 Hz, 4H, aryl-H), 7.41 (d, ⁴*J*_{HH} = 1.8 Hz, 4H, aryl-H). ¹³C{¹H} NMR (C₆D₆, 125.8 MHz) δ/ppm: 30.1 (-tBu), 32.1 (-tBu), 35.2 (-tBu), 35.4 (-tBu), 121.6 (aryl-C), 113.8 (aryl-C), 136.9 (aryl-C), 139.3 (aryl-C), 146.2 (aryl-C), 162.9 (aryl-C). APCI-MS (toluene) *m/z*: 1026.6 ([M]⁺), 1027.6 ([M+H]⁺). UV-vis (CH₂Cl₂) λ_{max} /nm (ε/M⁻¹ cm⁻¹): 286 (38,600), 378 (25,200), 420 (29,700).

Crystallographic Methods. X-ray diffraction data were collected on single crystals of W[SNS]₂ and W[ONO]₂ mounted on glass fibers using a Bruker CCD platform diffractometer equipped with a CCD detector. Measurements were carried out at 163 K using Mo Kα (λ = 0.71073 Å) radiation, which was wavelength selected with a single-crystal graphite monochromator. The SMART program package was used to determine unit-cell parameters and to collect data. The raw frame data were processed using SAINT and SADABS to yield the reflection data files. Subsequent calculations were carried out using the SHELXTL program suite. Structures were solved by direct methods

and refined on *F*² by full-matrix least-squares techniques. Analytical scattering factors for neutral atoms were used throughout the analyses.³⁵ Hydrogen atoms were included using a standard riding model. ORTEP diagrams were generated using ORTEP-3 for Windows.³⁶ Diffraction data for W[SNS]₂ and W[ONO]₂ are given in Table 1. Least-squared planes, trigonal twist angles, and prismatic compression values given in Table 3 were calculated using Mercury 3.0.

Table 1. X-ray Diffraction Data Collection and Refinement Parameters for W[SNS]₂ and W[ONO]₂

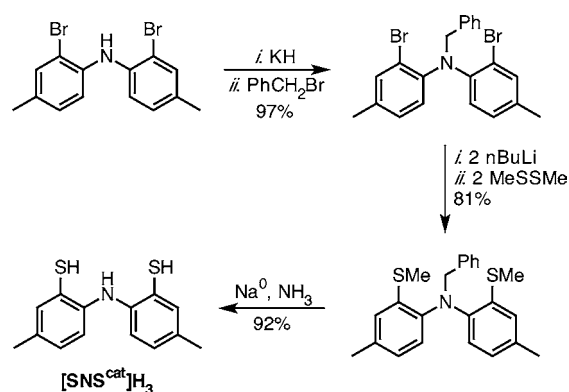
	W[SNS] ₂ ·C ₇ H ₈	W[ONO] ₂
empirical formula	C ₃₅ H ₃₂ N ₂ S ₄ W	C ₅₆ H ₈₀ N ₂ O ₄ W
formula weight	792.72	1029.07
crystal system	monoclinic	triclinic
space group	<i>P</i> 2 ₁ / <i>c</i>	<i>P</i> $\bar{1}$
<i>a</i> /Å	19.7206(6)	11.6164(7)
<i>b</i> /Å	10.6756(3)	12.0666(7)
<i>c</i> /Å	15.2817(5)	20.5721(12)
α /deg	90	82.7281(6)
β /deg	107.2028(3)	73.9437(6)
γ /deg	90	76.1399(6)
<i>V</i> /Å ³	3073.32(16)	2684.8(3)
<i>Z</i>	4	2
refl. collected	36891	31079
indep. refl.	7748	12287
R1 (<i>I</i> > 2σ) ^a	0.0151	0.0203
wR2 (all data) ^b	0.0351	0.0511

$${}^a R1 = \frac{\sum ||F_o| - |F_c||}{\sum |F_o|}. \quad {}^b wR2 = \left\{ \frac{\sum [w(F_o^2 - F_c^2)^2]}{\sum [w(F_o^2)]^2} \right\}^{1/2}.$$

RESULTS

Synthesis of [SNS^{cat}]₃H₃, W[SNS]₂, and W[ONO]₂. The tridentate ligand precursor bis(2-mercapto-*p*-tolyl)amine, [SNS^{cat}]₃H₃, was prepared in four scalable synthetic steps from commercially available di(*p*-tolyl)amine (Scheme 1).

Scheme 1



Bromination of the diarylamine derivative was achieved according to published procedures;³⁴ however, the product, as-isolated, required an additional purification step to be carried through the rest of the synthesis. Benzyl protection of the central nitrogen allowed the dibromide to be lithiated with *n*BuLi and subsequently oxidized with dimethyldisulfide to install the sulfur donors as methyl sulfide groups in *N*-benzyl-bis(2-methanethio-*p*-tolyl)amine. Simultaneous deprotection of both the benzylated nitrogen and the methylated sulfur atoms

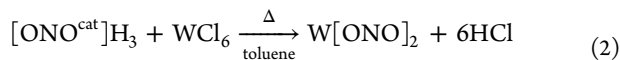
was achieved using Birch conditions³⁷ to afford the $[\text{SNS}^{\text{cat}}]\text{H}_3$ product in excellent yield as a yellow, viscous oil.

Metalation of the $[\text{SNS}^{\text{cat}}]\text{H}_3$ ligand was readily achieved using tungsten hexachloride (eq 1). The addition of yellow $[\text{SNS}^{\text{cat}}]\text{H}_3$ to a dark blue suspension of WCl_6 in toluene resulted in an immediate color change to dark maroon. To drive the reaction to completion via elimination of 6 equiv of HCl , the reaction mixture was heated to reflux for several hours. Shorter reaction times or reactions carried out at room temperature resulted in the sustained presence of protonated ligand resonances in the ^1H NMR spectrum indicative of incomplete product formation. The desired product, $\text{W}[\text{SNS}]_2$, was isolated as a purplish-brown solid from a mixture of toluene and pentane in 65% yield.



The new tungsten complex was identified to be the desired homoleptic $\text{W}[\text{SNS}]_2$ complex by a battery of analytical techniques. The APCI mass spectrum of $\text{W}[\text{SNS}]_2$ displayed overlapping peaks corresponding to $[\text{M}]^+$ and $[\text{M}+\text{H}]^+$ at 697.9 and 698.9 amu, respectively, with each signal displaying the expected isotopic distributions. ^1H and ^{13}C NMR spectra indicated D_{2d} symmetry for the complex in solution. A single methyl resonance in the ^1H NMR spectrum at 2.14 ppm was accompanied by three aryl proton resonances. The ^{13}C NMR spectrum showed the methyl carbon and six unique aryl carbon resonances in the 120–155 ppm region. In square-planar complexes of platinum(II) and palladium(II) containing the semiquinonate form of aminothiophenol ligands, $\text{M}(1,2\text{-C}_6\text{H}_6\text{SNR})_2$, ^{13}C NMR resonances were shifted to higher frequency, in the region 166–170 ppm.³⁸

Similar to the preparation of $\text{W}[\text{SNS}]_2$, the bis(phenolate) derivative, $\text{W}[\text{ONO}]_2$, was prepared from tungsten hexachloride and $[\text{ONO}^{\text{cat}}]\text{H}_3$ (eq 2). The bis[ONO] tungsten complex was isolated as an orange-brown solid in 74% yield from toluene upon addition of acetonitrile. The APCI mass spectrum of $\text{W}[\text{ONO}]_2$ displayed $[\text{M}]^+$ and $[\text{M}+\text{H}]^+$ peaks at 1026.7 and 1027.7 amu, respectively. Similar to $\text{W}[\text{SNS}]_2$, the $\text{W}[\text{ONO}]_2$ derivative displayed D_{2d} symmetry in both the ^1H and ^{13}C NMR spectra. Notably, the C–O carbon of $\text{W}[\text{ONO}]_2$ resonated at 162.9 ppm in the ^{13}C NMR spectrum, consistent with the resonance for that carbon in complexes of the fully reduced $[\text{ONO}^{\text{cat}}]^{3-}$ ligand.^{39–41}



Structures of $\text{W}[\text{SNS}]_2$ and $\text{W}[\text{ONO}]_2$. Single-crystal X-ray diffraction was used to establish the molecular structure of $\text{W}[\text{SNS}]_2$. X-ray quality single crystals of $\text{W}[\text{SNS}]_2$ were grown from a saturated toluene/acetonitrile solution of the complex chilled to -35°C . The complex crystallized in the monoclinic spacegroup $P2_1/c$, and the asymmetric unit contained one crystallized toluene molecule. Figure 1 shows the molecular structure of $\text{W}[\text{SNS}]_2$ and Table 2 contains selected metrical parameters for the structure.

Neither [SNS] ligand in six-coordinate $\text{W}[\text{SNS}]_2$ can be described as planar. The nitrogen atom in each [SNS] ligand displays planar, sp^2 hybridization (359° sum of angles around N); however, the ligand aryl rings are not coplanar. Defining the aryl rings of the [SNS] ligands as Π_n according to the attached sulfur atom, $\text{S}(n)$ (see Figure 2a), the intraligand angles between the aryl rings are $\angle(\Pi_1\text{--N}(1)\text{--}\Pi_2) = 46^\circ$ and

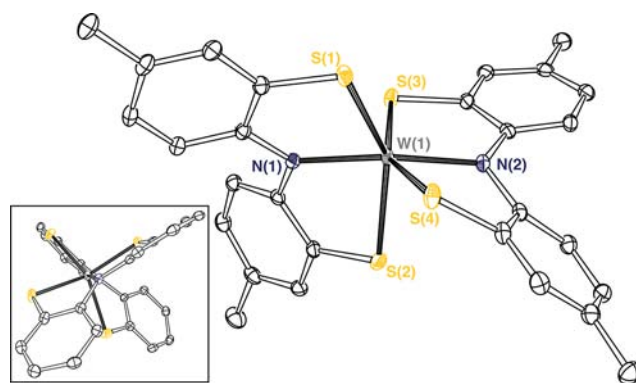


Figure 1. ORTEP diagram of $\text{W}[\text{SNS}]_2$. Ellipsoids are shown at 50% probability. Hydrogen atoms and a toluene molecule have been omitted for clarity. Inset: Core structure of $\text{W}[\text{SNS}]_2$ viewed along $\text{N}(1)\text{--W}(1)\text{--N}(2)$.

Table 2. Selected Bond Distances (Å) and Angles (deg) for $\text{W}[\text{ENE}]_2$ (E = S, O)

	$\text{W}[\text{SNS}]_2$	$\text{W}[\text{ONO}]_2$
Bond Distances/Å		
W(1)–E(1)	2.3942(4)	1.9057(13)
W(1)–E(2)	2.3718(4)	1.9061(13)
W(1)–E(3)	2.3296(4)	1.9123(13)
W(1)–E(4)	2.3732(4)	1.9130(13)
W(1)–N(1)	2.0592(14)	2.0449(15)
W(1)–N(2)	2.0843(13)	2.0380(15)
E(1)–C(2)	1.7310(17)	1.363(2)
E(2)–C(16/9)	1.7545(17)	1.365(2)
E(3)–C(30/16)	1.7463(17)	1.363(2)
E(4)–C(44/23)	1.7385(18)	1.365(2)
N(1)–C(1)	1.396(2)	1.416(2)
N(1)–C(15/8)	1.418(2)	1.415(3)
N(2)–C(29/15)	1.415(2)	1.413(2)
N(2)–C(43/22)	1.410(2)	1.413(2)
C(1)–C(2)	1.410(2)	1.400(3)
C(15/8)–C(16/9)	1.404(2)	1.402(3)
C(29/15)–C(30/16)	1.396(2)	1.401(3)
C(43/22)–C(44/23)	1.405(2)	1.401(2)
Bond Angles/deg		
N(1)–W(1)–E(1)	78.76(4)	76.55(6)
N(1)–W(1)–E(2)	79.41(4)	76.54(6)
N(2)–W(1)–E(3)	80.09(4)	76.37(6)
N(2)–W(1)–E(4)	77.82(4)	76.53(6)
N(1)–W(1)–N(2)	155.27(5)	175.81(6)
E(1)–W(1)–E(2)	145.170(16)	152.82(6)
E(3)–W(1)–E(4)	152.646(15)	152.87(6)

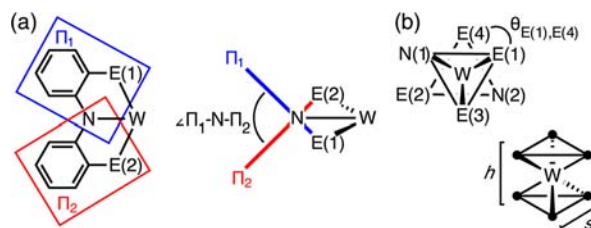


Figure 2. Diagrams of metrical parameters calculated for $\text{W}[\text{SNS}]_2$ (E = S) and $\text{W}[\text{ONO}]_2$ (E = O).

$\angle(\Pi_3\text{--N}(2)\text{--}\Pi_4) = 38^\circ$. As shown in the inset of Figure 1, these distortions from planarity within the [SNS] ligand

manifest a distorted geometry for the tungsten center. The N(1)–W–N(2) bond angle of 155° is significantly smaller than that expected for an octahedral complex. Intraligand S–W–S angles are 145° and 153° while interligand S–W–S angles vary from 80° to 105° . It should be noted that while interligand S–S bond formation has been observed in complexes with ONS chelating ligands,²⁴ in the case of W[SNS]₂, all S...S distances are greater than 3.05 Å.

The overall tungsten geometry in W[SNS]₂ is in between trigonal prismatic and trigonal antiprismatic (pseudo-octahedral).⁴² The primary measure of prismatic versus antiprismatic geometry is the twist angle (θ) between opposite trigonal faces (Figure 2b). In W[SNS]₂, the two trigonal planes can be defined by the nitrogen and one sulfur atom from one [SNS] ligand and a sulfur atom from the other ligand (N(1)–S(1)–S(3) and N(2)–S(2)–S(4)), and the twist angle is then defined as the torsion angle between the vertices of the trigonal planes and the centroids of those planes. In an ideal trigonal prism, $\theta = 0^\circ$ whereas in an antiprism, $\theta = 60^\circ$.⁴² A second metrical parameter used to differentiate trigonal prismatic and trigonal antiprismatic geometries is the prismatic compression, defined as the ratio of the prism height, h , to the (average) length of the trigonal face, s . For an ideal trigonal prism $s/h = 1.00$, whereas in an ideal octahedron $s/h = 1.22$.⁴² Table 3

Table 3. Additional Measured and Calculated Metrical Parameters for W[SNS]₂ and W[ONO]₂, As Defined in Figure 2^a

	W[SNS] ₂ ·C ₇ H ₈	W[ONO] ₂
$\angle \Pi_1$ –N(1)– Π_2	46.5	6.0
$\angle \Pi_3$ –N(2)– Π_4	38.0	10.6
$\theta_{E(1), E(4)}$	10.2	35.3
$\theta_{N(1), E(2)}$	27.4	47.1
$\theta_{E(3), N(2)}$	33.4	45.2
s/h	1.11	1.23

^aThe plane defined by the six carbon atoms of each (thio)phenolate moiety are indicated by Π_n , where “ n ” is the number of the attached atom E (E = S, O).

summarizes the twist angles and prismatic compression values for W[SNS]₂ as determined from the single crystal X-ray data. Both parameters fall midway between the expected values for a trigonal prism and a trigonal antiprism.

Examination of the extended solid state structure of W[SNS]₂ revealed intermolecular contacts between the aryl groups of the [SNS] ligand, as illustrated in Figure 3. Three of

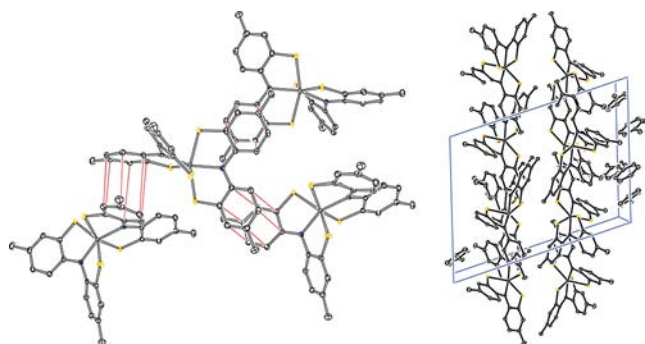


Figure 3. Left: Diagram highlighting the π – π interactions in the solid state structure of W[SNS]₂. Right: The unit cell of W[SNS]₂.

the aryl rings in each W[SNS]₂ molecule are in close contact (<3.7 Å) with nearby aryl rings on adjacent molecules, setting up π – π stacking interactions.^{43,44} The Π_1 and Π_4 rings stack at a distance of 3.64 Å from adjacent Π_4 and Π_1 rings, respectively, whereas the Π_3 ring stacks at a distance of 3.53 Å from an adjacent Π_3 ring. Only the Π_2 ring lacks intermolecular π – π stacking interactions.

The bond distances for W[SNS]₂ are consistent with a partially oxidized [SNS] ligand. The average W–S distance of 2.37 Å is similar to those observed in W(pdt)₃ and [W(pdt)₃][–] (pdt^{2–} = 1,2-diphenyl-1,2-dithiolate), which were recently described as W^V and W^{IV} complexes, respectively, with partially oxidized dithiolene ligands.⁴⁵ The average C–N and C–S distances in W[SNS]₂ are 1.41 and 1.74 Å, respectively. In bidentate ortho-aminothiophenolate ligands, the catecholate oxidation state is characterized by C–N and C–S distances of 1.41 and 1.76 Å, respectively, whereas the semiquinonate oxidation state is characterized by C–N and C–S distances of 1.36 and 1.72 Å, respectively.^{24,38,46,47} Oxidized ortho-aminothiophenolate ligands also display partial localization of double-bond character within the aryl rings with differences between the longest and shortest C–C bonds, (ΔC)_{max} of about 0.06 Å. In W[SNS]₂, partial double bond localization is evident from (ΔC)_{max} values ranging from 0.015 to 0.04 Å for the four aryl rings.

In contrast to the structure of W[SNS]₂, the single-crystal X-ray diffraction analysis of W[ONO]₂ revealed a pseudo-octahedral environment around the tungsten center with nearly planar [ONO] ligands. The molecular structure of W[ONO]₂ is shown in Figure 4, and the corresponding metrical

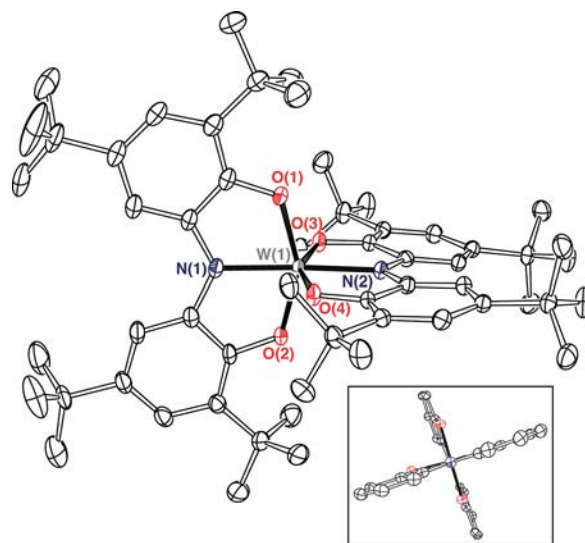


Figure 4. ORTEP diagram of W[ONO]₂. Ellipsoids are shown at 50% probability. Hydrogen atoms have been omitted for clarity. Inset: Core structure of W[ONO]₂ viewed along N(1)–W(1)–N(2).

parameters for W[ONO]₂ are provided in Tables 2 and 3. Single crystals of W[ONO]₂ were grown by evaporation of solvent from a saturated CH₂Cl₂ solution of the complex. The geometry around the tungsten center of W[ONO]₂ is consistent with a trigonal antiprism with the two [ONO] ligands perpendicular to one another given an average interligand O–W–O bond angle of 93.15° and an N(1)–W–N(2) angle of 176° . The meridional binding of the [ONO] ligands give rise to nearly coplanar intraligand aryl rings. As

shown in Table 3, the $\Pi_1-N(1)-\Pi_2$ and $\Pi_3-N(2)-\Pi_4$ angles are only 6° and 11° , respectively. Trigonal twist angles for $W[ONO]_2$ are larger than those measured for $W[SNS]_2$ (Table 3); however, the limited bite angle of the [ONO] ligand platform still keeps these values shy of the ideal value for a trigonal antiprism. Nevertheless, a prismatic compression value of 1.23 is consistent with an antiprismatic structure.

Ligand oxidation states for $W[ONO]_2$ are readily assigned from the high-resolution X-ray data. The average tungsten–oxygen distance of 1.91 Å is comparable to those in octahedral $W(O-p\text{-tolyl})_6$ ($W-O_{\text{ave}} = 1.90$ Å) and $W(O_2C_2Me_4)_3$ ($W-O_{\text{ave}} = 1.91$ Å).^{48,49} Within the [ONO] ligands, C–N and C–O distances of 1.41 and 1.36 Å, respectively, are entirely consistent with the C–N and C–O distances observed in $[ONO^{\text{cat}}]Ta^VCl_2(OEt_2)$ and $[ONO^{\text{cat}}]Zr^{IV}Cl(THF)_2$ complexes.^{1,50} The aryl rings of the ligand show no signs of localized double-bonds, which would be expected for an oxidized ligand.

Spectroscopic and Electrochemical properties of $W[SNS]_2$ and $W[ONO]_2$. The electronic absorption spectra of $W[SNS]_2$ and $W[ONO]_2$, shown in Figure 5, are dominated

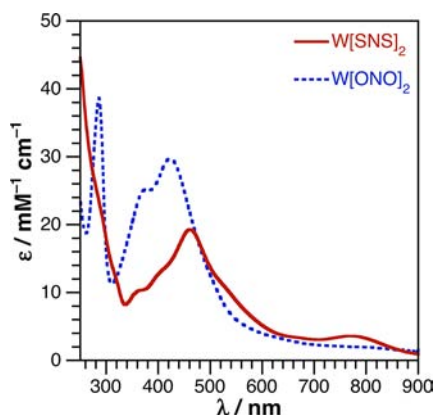


Figure 5. UV–vis absorption spectra for $W[SNS]_2$ and $W[ONO]_2$ in CH_2Cl_2 .

by intense transitions in the UV–visible region of the spectrum. The dominant absorption of $W[SNS]_2$ is centered at 461 nm ($\epsilon = 19,300 \text{ M}^{-1} \text{ cm}^{-1}$) with shoulders on both sides of the maximum. A lower intensity transition can be seen at 766 nm ($\epsilon = 3,620 \text{ M}^{-1} \text{ cm}^{-1}$). These absorption energies and intensities are similar to those observed for tris(dithiolene) complexes of tungsten such as $W[bdt]_3$ and $W[tbbdt]_3$ ($bdt^{2-} = \text{benzene-1,2-dithiolate}$; $tbbdt^{2-} = 3,5\text{-di-}tert\text{-butylbenzene-1,2-dithiolate}$).^{45,51} The $W[ONO]_2$ derivative has better resolved optical features with a sharp, high-energy absorption at 286 nm ($\epsilon = 45,100 \text{ M}^{-1} \text{ cm}^{-1}$) and two overlapping absorptions at 378 and 420 nm ($\epsilon = 25,200$ and $29,700 \text{ M}^{-1} \text{ cm}^{-1}$, respectively). The electronic absorption spectrum of $W[ONO]_2$ is quite different than the spectra reported for other homoleptic, transition-metal complexes, $M[ONO]_2$ ($M = \text{Ti, Fe, Mn, Co, Ni, Cu}$), which typically contain one or more oxidized [ONO] ligands and display intense absorptions in the 700–1000 nm wavelength region.^{9,11,12}

Cyclic voltammetry studies of $W[SNS]_2$ and $W[ONO]_2$ revealed multiple one-electron reductive and oxidative processes. Figure 6 shows cyclic voltammogram traces for $W[SNS]_2$ and $W[ONO]_2$; the scan rate dependencies of the cyclic voltammetry data are provided as Supporting Informa-

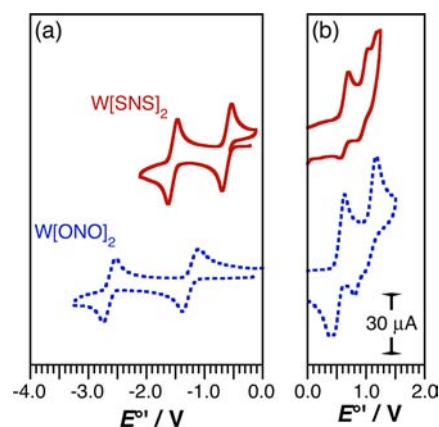


Figure 6. Cyclic voltammograms of $W[SNS]_2$ and $W[ONO]_2$ in (a) THF and (b) CH_2Cl_2 . Measurements were made under N_2 using a scan rate of 200 mV s^{-1} on 1.0 mM analyte solutions containing 0.10 M $[Bu_4N][PF_6]$ electrolyte. Potentials were referenced to $[Cp_2Fe]^{+/0}$ using an internal standard.

tion. The electrochemical behavior of the complexes was similar in THF, MeCN, and CH_2Cl_2 . While the oxidations of both $W[SNS]_2$ and $W[ONO]_2$ were best observed in CH_2Cl_2 , the second reduction of $W[ONO]_2$ was too negative to be observed in the CH_2Cl_2 solvent window. Thus, the cathodic portion of the cyclic voltammograms of Figure 6 were acquired in THF while the anodic portion of the cyclic voltammograms of Figure 6 were acquired in CH_2Cl_2 . The measured potentials for $W[SNS]_2$ and $W[ONO]_2$, referenced to $[Cp_2Fe]^{+/0}$ using an internal standard, are listed in Table 4. The $W[SNS]_2$

Table 4. Electrochemical Data for $W[SNS]_2$ and $W[ONO]_2$ ^a

	$E_{1}^{o'}$ ($[M]^{1-/2-}$) ^b	$E_{2}^{o'}$ ($[M]^{0/1-}$) ^b	$E_{3pa}^{o'}$ ($[M]^{2+/0}$) ^c	$E_{4pa}^{o'}$ ($[M]^{2+/1+}$) ^c
$W[SNS]_2$	-1.55	-0.61	0.70	1.05
$W[ONO]_2$	-2.77	-1.38	0.63	1.16

^aPotentials were referenced to $[Cp_2Fe]^{+/0}$ using an internal standard. ^b1.0 mM analyte in THF containing 0.1 M $[Bu_4N][PF_6]$. ^c1.0 mM analyte in CH_2Cl_2 containing 0.1 M $[Bu_4N][PF_6]$.

complex displays two reductive and two oxidative processes. Based on the relative intensities for these signals, all four processes appear to be single electron in nature. While the reductive processes for $W[SNS]_2$ appear to be reversible ($i_{pa}/i_{pc} \approx 1.0$), the oxidative processes do not display significant reversible character. The two reductions of $W[SNS]_2$ are separated by 0.94 V.

The electrochemical data for $W[ONO]_2$ is significantly different from that recorded for the sulfur homologue. $W[ONO]_2$ displays two reversible reductions that are shifted cathodically relative to the reductions in $W[SNS]_2$; moreover, the two reductions are separated by almost 1.4 V. In the anodic portion of the voltammogram, $W[ONO]_2$ displays two oxidative processes that are at least partially reversible. It is noteworthy that comparison of the peak intensities of the reductive and oxidative processes suggest that the oxidations may be two-electron in nature. This proposal is qualitatively supported by the plateaued cathodic portion of the first oxidation of $W[ONO]_2$, which shows two features at slow scan rates, and may be indicative of partial resolution of two one-electron processes.

DISCUSSION

The new redox-active pincer-type ligand precursor, [SNS]H₃, is readily accessible from commercially available diphenylamine derivatives. Installation of the sulfur donor atoms relied on an initial arene oxidation ortho to the amine functionality followed by lithiation and subsequent oxidation with dimethyldisulfide. While the synthetic route required four steps, including protection of the amine and deprotection of the amino and thiol groups, the steps proceed in high yields making the synthetic procedure viable for the preparation of the ligand in gram quantities. Furthermore, the procedure should work for other diphenylamine derivatives with substituents in the 4 and 4' position to guard against para bromination in the first reaction step.

The homoleptic W[SNS]₂ and W[ONO]₂ complexes were readily accessed by the reaction of appropriate ligand with WCl₆ to extrude HCl. ¹H NMR experiments indicated that relatively long reaction times (hours) and relatively high temperatures (refluxing toluene) were required to drive the reaction to completion. Under milder conditions, unidentified tungsten products were observed including species with a nitrogen-protonated [SNHS] ligand.

While W[ONO]₂ displayed a regular trigonal antiprismatic structure in the solid state, the structure of W[SNS]₂ proved to be an irregular six-coordinate species that is intermediate between trigonal prismatic and trigonal antiprismatic geometries. The reason for the distorted geometry in W[SNS]₂ is unclear. It could be attributed to packing effects stemming from the π - π stacking interactions observed in the solid-state structure. Alternatively, it is well-known that homoleptic tungsten thiolate complexes show a range of six-coordinate geometries.²³ Thus, the observed geometry of W[SNS]₂ may be a product of competing electronic factors that favor a trigonal prismatic structure²³ and steric limitations of a planar [SNS] ligand that favor an antiprismatic structure. While it might be expected that a partially oxidized [SNS] ligand should favor a planar ligand geometry, previous studies have shown that oxidation of thiolate ligands occurs primarily at the sulfur atom, with decreased delocalization of the resultant hole through the aromatic ring system.⁵² Another important caveat to rationalizing the solid-state structure is that on the NMR time scale there is no evidence for the unsymmetrical structure of W[SNS]₂ in solution. This result could result from either a more symmetrical and regular structure in solution (i.e., loss of π - π stacking interactions), or a fluxional coordination environment that averages inequivalent chemical positions.

Of particular interest here is a comparison of the electronic properties of the [SNS] and [ONO] ligand platforms, particularly their redox activity. In this respect, the two homoleptic complexes W[SNS]₂ and W[ONO]₂ provide a case study of the two ligand platforms.

The homoleptic W[ONO]₂ complex is best described as a W^{VI}[ONO^{cat}]₂ complex. The single crystal X-ray diffraction data for W[ONO]₂ shows W–O, O–C, and N–C bond distances that are consistent with a tungsten(VI) metal center coordinated to [ONO] ligands in the fully reduced, catecholate oxidation state. Furthermore, C–C bond distances within the [ONO] ligand show no evidence for the cyclohexadiene character manifested with ligand oxidation. In contrast, other homoleptic M[ONO]₂ complexes reported in the literature have been assigned to contain some combination of [ONO^{sq}]²⁻ and [ONO^q]⁻ ligands.^{8–10,12,15,53–58} The electro-

chemistry of W[ONO]₂ shows two one-electron reductions at very negative potentials and with a large peak-to-peak separation. These data are consistent with sequential reduction of a tungsten(VI) center first to tungsten(V) and then to tungsten(IV).^{59,60} Similarly negative first and second reduction potentials, with large peak-to-peak separations, have been observed for homoleptic aryloxides and catecholate complexes of tungsten. On the oxidative side, integration of the oxidative process at +0.63 V suggests that it is a two-electron process. Given a W^{VI}[ONO^{cat}]₂ electron configuration and an orthogonal arrangement of the [ONO] ligands, a two-electron oxidation could arise from coincident one-electron oxidations of each [ONO] ligand. It is worth noting that such an assignment implies that the cation W[ONO]₂⁺ would be a Robin–Day Class I mixed-valence complex,^{56,61} but more detailed electrochemical and spectroscopic analyses are required to confirm such a characterization.

Structural and electrochemical data for W[SNS]₂ suggest a subtly different electron distribution from that of W[ONO]₂. In W[SNS]₂, better spatial and energetic overlap between the tungsten d orbitals and sulfur p lone-pair orbitals would lead to a more pronounced π interaction between the metal and [SNS] ligand. In the limit of purely covalent π bonding between the tungsten center and the [SNS] ligand, the experimental metal and ligand oxidation states would be best described as W^{IV}[SNS^{sq}]₂. It is important to note that this oxidation state assignment does not require any radical (or diradical) character in W[SNS]₂. Instead, it is only meant to imply equal sharing between the tungsten center and the two [SNS] ligands of two electron pairs in two perpendicular π orbitals. This electronic structure assignment is consistent with studies of tungsten tris(dithiolene) complexes, which have been assigned as W^{IV} or W^V species coordinated by a mixture of dianionic and monoanionic dithiolenes.^{23,45,62–65} While the structural differences observed for W[SNS]₂ are too small for an unequivocal assignment of metal and ligand oxidation states, especially given the irregular solid-state geometry of the complex, the W–S and S–C bond distances are consistent with a partially oxidized [SNS] ligand. Similarly, while the electrochemistry of W[SNS]₂ is superficially similar to that of W[ONO]₂, subtle differences suggest a different frontier electronic configuration for the sulfur derivative. Two reversible, one-electron reductions are observed for W[SNS]₂, but they occur at significantly milder potentials than the reductions observed for W[ONO]₂, and they are separated by only 0.94 V. This result is surprising since simple electronegativity arguments would suggest that the oxygen-containing, [ONO] derivative would be easier to reduce than the sulfur-containing, [SNS] derivative. Within the model of a W^{IV}[SNS^{sq}]₂ electron configuration, each reduction would add an electron to a molecular orbital delocalized over the tungsten metal and [SNS] ligand; therefore, electron–electron repulsion would be smaller owing to the delocalized nature of these orbitals leading to less negative reduction potentials. For the oxidation of W[SNS]₂, the electrochemical processes are less well-resolved, and less reversible than for W[ONO]₂, but there is no indication that they are two-electron processes. Similarly, oxidations of tris(dithiolene) complexes of tungsten are also irreversible, which has been attributed to unprotected sulfur atoms with significant radical character.⁵¹ Within the W^{IV}[SNS^{sq}]₂ model, the oxidations would again come from molecular orbitals delocalized over the tungsten metal and [SNS] ligands, resulting in significant radical character on the sulfur atoms.

SUMMARY

The new amidedithiolate ligand, $[\text{SNS}^{\text{cat}}]^{3-}$, offers a redox-active ligand platform for the preparation of coordination complexes. Structural and electrochemical studies suggest that the $[\text{SNS}]$ platform maintains similar redox properties to the well-established $[\text{ONO}]$ ligand, but whereas the hard oxygen and nitrogen donors of $[\text{ONO}]$ favor a $\text{W}^{\text{VI}}[\text{ONO}^{\text{cat}}]_2$ electronic structure, the softer sulfur donor atoms of the $[\text{SNS}]$ ligand seem to increase metal–ligand covalency in the π -bonding manifold, increasing the $\text{W}^{\text{IV}}[\text{SNS}^{\text{sq}}]_2$ character of the complex. Because the $[\text{SNS}]$ ligand is readily prepared in good yields, and since metalation is straightforward, the $[\text{SNS}]$ ligand should receive considerable attention for the preparation of new coordination complexes in which ligand-based redox-activity, meridional binding, and softer donor atoms are desirable. Given the importance of sulfur-based ligands in metalloenzymes, the tridentate $[\text{SNS}]$ ligand offers a new platform for pursuing reactivity models for various hydroxylase, reductase, and oxygen-atom transfer enzymes.

ASSOCIATED CONTENT

Supporting Information

X-ray crystallographic data for $\text{W}[\text{SNS}]_2 \cdot \text{C}_6\text{H}_5\text{Me}$ and $\text{W}[\text{ONO}]_2$ (CIF format); ^1H and ^{13}C NMR data for $\text{W}[\text{SNS}]_2$ and $\text{W}[\text{ONO}]_2$, and full cyclic voltammograms of $\text{W}[\text{SNS}]_2$ and $\text{W}[\text{ONO}]_2$ in both THF and CH_2Cl_2 (PDF format). This material is available free of charge via the Internet at <http://pubs.acs.org>.

AUTHOR INFORMATION

Corresponding Author

*E-mail: aheyduk@uci.edu.

Notes

The authors declare no competing financial interest.

ACKNOWLEDGMENTS

The authors acknowledge the National Science foundation for supporting this work (CHE-1152543). A.F.H. is a Camille Dreyfus Teacher-Scholar.

REFERENCES

- Heyduk, A. F.; Zarkesh, R. A.; Nguyen, A. I. *Inorg. Chem.* **2011**, *50*, 9849–9863.
- van der Vlugt, J. I.; Reek, J. N. *Angew. Chem., Int. Ed.* **2009**, *48*, 8832–8846.
- Gibson, V. C.; Redshaw, C.; Solan, G. A. *Chem. Rev.* **2007**, *107*, 1745–1776.
- Ivakhnenko, E. P.; Starikov, A. G.; Minkin, V. I.; Lyssenko, K. A.; Antipin, M. Y.; Simakov, V. I.; Korobov, M. S.; Borodkin, G. S.; Knyazev, P. A. *Inorg. Chem.* **2011**, *50*, 7022–7032.
- Adhikari, D.; Mossin, S.; Basuli, F.; Huffman, J. C.; Szilagy, R. K.; Meyer, K.; Mindiola, D. J. *J. Am. Chem. Soc.* **2008**, *130*, 3676–3682.
- Herbert, D. E.; Ozerov, O. V. *Organometallics* **2011**, *30*, 6641–6654.
- Wanniarachchi, S.; Liddle, B. J.; Kizer, B.; Hewage, J. S.; Lindeman, S. V.; Gardinier, J. R. *Inorg. Chem.* **2012**, *51*, 10572–10580.
- Brown, M. A.; Castro, J. A.; McGarvey, B. R.; Tuck, D. G. *Can. J. Chem.* **1999**, *77*, 502–510.
- Bruni, S.; Caneschi, A.; Cariati, F.; Delfs, C.; Dei, A.; Gatteschi, D. *J. Am. Chem. Soc.* **1994**, *116*, 1388–1394.
- Camacho-Camacho, C.; Merino, G.; Martinez-Martinez, F. J.; Noth, H.; Contreras, R. *Eur. J. Inorg. Chem.* **1999**, 1021–1027.
- Girgis, A. Y.; Balch, A. L. *Inorg. Chem.* **1975**, *14*, 2724–2727.

- Larsen, S. K.; Pierpont, C. G. *J. Am. Chem. Soc.* **1988**, *110*, 1827–1832.
- McGarvey, B. R.; Ozarowski, A.; Tian, Z.; Tuck, D. G. *Can. J. Chem.* **1995**, *73*, 1213–1222.
- Simpson, C. L.; Boone, S. R.; Pierpont, C. G. *Inorg. Chem.* **1989**, *28*, 4379–4385.
- Speier, G.; Csihony, J.; Whalen, A. M.; Pierpont, C. G. *Inorg. Chem.* **1996**, *35*, 3519–3524.
- Chaudhuri, P.; Hess, M.; Weyhermüller, T.; Wiegardt, K. *Angew. Chem., Int. Ed.* **1999**, *38*, 1095–1098.
- Szigethy, G.; Shaffer, D. W.; Heyduk, A. F. *Inorg. Chem.* **2012**, *51*, 12606–12618.
- Davison, A.; Edelstein, N.; Holm, R. H.; Maki, A. H. *J. Am. Chem. Soc.* **1963**, *85*, 2029–2030.
- Gray, H. B.; Williams, R.; Bernal, I.; Billig, E. *J. Am. Chem. Soc.* **1962**, *84*, 3596–3597.
- Schrauzer, G. N.; Mayweg, V. *J. Am. Chem. Soc.* **1962**, *84*, 3221–3221.
- Stiefel, E. I.; Waters, J. H.; Billig, E.; Gray, H. B. *J. Am. Chem. Soc.* **1965**, *87*, 3016–3017.
- McCleverty, J. A. *Prog. Inorg. Chem.* **1968**, *10*, 49–221.
- Eisenberg, R. *Coord. Chem. Rev.* **2010**, *255*, 825–836.
- Roy, N.; Sproules, S.; Weyhermüller, T.; Wiegardt, K. *Inorg. Chem.* **2009**, *48*, 3783–3791.
- Hübner, R.; Weber, S.; Strobel, S.; Sarkar, B.; Zálaiš, S.; Kaim, W. *Organometallics* **2011**, *30*, 1414–1418.
- Ye, S.; Sarkar, B.; Lissner, F.; Schleid, T.; van Slageren, J.; Fiedler, J.; Kaim, W. *Angew. Chem., Int. Ed.* **2005**, *44*, 2103–2106.
- Noveron, J. C.; Olmstead, M. M.; Mascharak, P. K. *Inorg. Chem.* **1998**, *37*, 1138–1139.
- Wong, Y.-L.; Dilworth, J. R. *Dalton Trans.* **2002**, 2366–2370.
- Takemoto, S.; Kawamura, H.; Yamada, Y.; Okada, T.; Ono, A.; Yoshikawa, E.; Mizobe, Y.; Hidai, M. *Organometallics* **2002**, *21*, 3897–3904.
- Xiao, J.; Deng, L. *Organometallics* **2011**, *31*, 428–434.
- Harkins, S. B.; Peters, J. C. *J. Am. Chem. Soc.* **2004**, *126*, 2885–2893.
- Hahn, R.; Nakamura, A.; Tanaka, K.; Nakayama, Y. *Inorg. Chem.* **1995**, *34*, 6562–6564.
- Connelly, N. G.; Geiger, W. E. *Chem. Rev.* **1996**, *96*, 877–910.
- Corey, J. Y.; Trankler, K. A.; Braddock-Wilking, J.; Rath, N. P. *Organometallics* **2010**, *29*, 5708–5713.
- International Tables for X-ray Crystallography*; Kluwer Academic: Dordrecht, The Netherlands, 1992.
- Farrugia, L. J. *J. Appl. Crystallogr.* **1997**, *30*, 565–565.
- Kumar, S.; Jaller, D.; Patel, B.; LaLonde, J. M.; DuHadaway, J. B.; Malachowski, W. P.; Prendergast, G. C.; Muller, A. J. *J. Med. Chem.* **2008**, *51*, 4968–4977.
- Herebian, D.; Bothe, E.; Bill, E.; Weyhermüller, T.; Wiegardt, K. *J. Am. Chem. Soc.* **2001**, *123*, 10012–10023.
- Zarkesh, R. A.; Ziller, J. W.; Heyduk, A. F. *Angew. Chem., Int. Ed.* **2008**, *47*, 4715–4718.
- Zarkesh, R. A.; Heyduk, A. F. *Organometallics* **2009**, *28*, 6629–6631.
- Zarkesh, R. A.; Heyduk, A. F. *Organometallics* **2011**, *30*, 4890–4898.
- Stiefel, E. I.; Brown, G. F. *Inorg. Chem.* **1972**, *11*, 434–436.
- Hunter, C. A.; Sanders, J. K. M. *J. Am. Chem. Soc.* **1990**, *112*, 5525–5534.
- Janiak, C. *Dalton Trans.* **2000**, 3885–3896.
- Sproules, S.; Banerjee, P.; Weyhermüller, T.; Yan, Y.; Donahue, J. P.; Wiegardt, K. *Inorg. Chem.* **2011**, *50*, 7106–7122.
- Ghosh, P.; Begum, A.; Herebian, D.; Bothe, E.; Hildenbrand, K.; Weyhermüller, T.; Wiegardt, K. *Angew. Chem., Int. Ed.* **2003**, *42*, 563–567.
- Sproules, S.; Wiegardt, K. *Coord. Chem. Rev.* **2011**, *255*, 837–860.
- Clegg, W.; Errington, R. J.; Kraxner, P.; Redshaw, C. *Dalton Trans.* **1992**, 1431–1438.

- (49) Lehtonen, A.; Sillanpää, R. *Polyhedron* **1994**, *13*, 2519–2524.
- (50) Lu, F.; Zarkesh, R. A.; Heyduk, A. F. *Eur. J. Inorg. Chem.* **2012**, 467–470.
- (51) Kapre, R. R.; Bothe, E.; Weyhermüller, T.; DeBeer George, S.; Wieghardt, K. *Inorg. Chem.* **2007**, *46*, 5642–5650.
- (52) Bachler, V.; Olbrich, G.; Neese, F.; Wieghardt, K. *Inorg. Chem.* **2002**, *41*, 4179–4193.
- (53) Caneschi, A.; Cornia, A.; Dei, A. *Inorg. Chem.* **1998**, *37*, 3419–3421.
- (54) Chaudhuri, P.; Hess, M.; Hildenbrand, K.; Bill, E.; Weyhermueller, T.; Wieghardt, K. *Inorg. Chem.* **1999**, *38*, 2781–2790.
- (55) Evangelio, E.; Bonnet, M.-L.; Cabanaser, M.; Nakano, M.; Sutter, J.-P.; Dei, A.; Robert, V.; Ruiz-Molina, D. *Chem.—Eur. J.* **2010**, *16*, 6666–6677.
- (56) Brunschwig, B. S.; Creutz, C.; Sutin, N. *Chem. Soc. Rev.* **2002**, *31*, 168–184.
- (57) Ruiz-Molina, D.; Veciana, J.; Wurst, K.; Hendrickson, D. N.; Rovira, C. *Inorg. Chem.* **2000**, *39*, 617–619.
- (58) Simpson, C. L.; Boone, S. R.; Pierpont, C. G. *Inorg. Chem.* **1989**, *28*, 4379–4385.
- (59) Beshouri, S. M.; Rothwell, I. P. *Inorg. Chem.* **1986**, *25*, 1962–1964.
- (60) Sydora, O. L.; Goldsmith, J. I.; Vaid, T. P.; Miller, A. E.; Wolczanski, P. T.; Abruña, H. D. *Polyhedron* **2004**, *23*, 2841–2856.
- (61) Robin, M. B.; Day, P. *Adv. Inorg. Chem. Radiochem.* **1967**, *10*, 247–422.
- (62) Enemark, J. H.; Cooney, J. J. A.; Wang, J.-J.; Holm, R. H. *Chem. Rev.* **2003**, *104*, 1175–1200.
- (63) Huynh, H.; Lügger, T.; Hahn, F. E. *Eur. J. Inorg. Chem.* **2002**, 3007–3009.
- (64) Sugimoto, H.; Tsukube, H. *Chem. Soc. Rev.* **2008**, *37*, 2609–2619.
- (65) Sung, K.-M.; Holm, R. H. *Inorg. Chem.* **2001**, *40*, 4518–4525.